The Journal of Chemical Physics ARTICLE scitation.org/journal/jcp

Anomalous temperature dependence of the experimental x-ray structure factor of supercooled water

Cite as: J. Chem. Phys. 155, 214501 (2021); doi: 10.1063/5.0075499
Submitted: 15 October 2021 • Accepted: 8 November 2021 •
Published Online: 1 December 2021

Niloofar Esmaeildoost,[1] Harshad Pathak,[2] Alexander Späh,[2] Thomas J. Lane,[3] Kyung Hwan Kim,[4] Cheolhee Yang,[4] Katrin Amann-Winkel,[2] Marjorie Ladd-Parada,[2] Fivos Perakis,[2] Jayanath Koliyadu,[5] Alexander R. Oggenfuss,[6] Philip J. M. Johnson,[6] Yunpei Deng,[6] Serhane Zerdane,[6] Roman Mankowsky,[6] Paul Beaud,[6] Henrik T. Lemke,[6] Anders Nilsson,[2] and Jonas A. Sellberg[1,a)]

AFFILIATIONS

[1] Biomedical and X-ray Physics, Department of Applied Physics, AlbaNova University Center, KTH Royal Institute of Technology, S-106 91 Stockholm, Sweden
[2] Department of Physics, AlbaNova University Center, Stockholm University, S-106 91 Stockholm, Sweden
[3] Linac Coherent Light Source, SLAC National Accelerator Laboratory, Menlo Park, California 94025, USA
[4] Department of Chemistry, Pohang University of Science and Technology, Pohang 37673, Republic of Korea
[5] European XFEL, 22869 Schenefeld, Germany
[6] SwissFEL, Paul Scherrer Institute, CH-5232 Villigen, Switzerland

[a)] **Author to whom correspondence should be addressed:** jonassel@kth.se

ABSTRACT

The structural changes of water upon deep supercooling were studied through wide-angle x-ray scattering at SwissFEL. The experimental setup had a momentum transfer range of 4.5 $Å^{-1}$, which covered the principal doublet of the x-ray structure factor of water. The oxygen–oxygen structure factor was obtained for temperatures down to 228.5 ± 0.6 K. Similar to previous studies, the second diffraction peak increased strongly in amplitude as the structural change accelerated toward a local tetrahedral structure upon deep supercooling. We also observed an anomalous trend for the second peak position of the oxygen–oxygen structure factor (q_2). We found that q_2 exhibits an unprecedented positive partial derivative with respect to temperature for temperatures below 236 K. Based on Fourier inversion of our experimental data combined with reference data, we propose that the anomalous q_2 shift originates from that a repeat spacing in the tetrahedral network, associated with all peaks in the oxygen–oxygen pair-correlation function, gives rise to a less dense local ordering that resembles that of low-density amorphous ice. The findings are consistent with that liquid water consists of a pentamer-based hydrogen-bonded network with low density upon deep supercooling.

I. INTRODUCTION

Water is the main constituent of Earth's hydrosphere and thus plays a central role in a wide range of scientific disciplines. Its physical properties are most well-studied among liquids and exhibit many anomalies despite the simplicity of the molecule. In particular, its thermodynamic response functions invert their simple behavior at high temperatures with monotonically decreasing magnitude upon cooling and increase quickly in magnitude upon deep supercooling. This counterintuitive behavior of increasing volume and entropy fluctuations upon supercooling has been connected to various thermodynamic scenarios[1,2] that can be summarized in Landau theory applied to fluid polymorphism[3] but has also been interpreted as a non-equilibrium phenomenon manifesting ice coarsening.[4–6]

Numerous experimental techniques have been applied to learn more about the origin of the anomalous behavior of the thermodynamic response functions of water. Nevertheless, it has always been

a challenge to measure these functions upon deep supercooling. X-ray scattering has emerged as one of the major techniques to study metastable water structures and extract correlation lengths. Small-angle x-ray scattering (SAXS), using an Ornstein–Zernike framework, has been used to determine the correlation length[7–9] of the metastable liquid. Although the correlation length is far from divergence,[7] maxima in correlation length,[9] isothermal compressibility,[9] and specific heat capacity[10] have been found at about 230 K. The increase in volume and entropy fluctuations coincides with an accelerated growth of local tetrahedral structures.[9,11] This is inferred from wide-angle x-ray scattering (WAXS) for which the momentum transfer covers the principal doublet (i.e., first two peaks) of the x-ray structure factor.[11,12]

The structure factor of water has been studied extensively with x-rays as well as neutrons under ambient conditions, and a benchmark oxygen–oxygen pair-correlation function, $g_{OO}(r)$, has been derived[13,14] with associated uncertainties. Water close to the boiling point shows a broad diffraction peak at about 2.5 Å^{-1} in the x-ray structure factor.[12] This feature splits into two well-defined maxima (doublet) that separate further apart upon cooling. Upon supercooling, Skinner *et al.*[12] confirmed a linear trend in the increased splitting of the doublet, which has been correlated with the amplitude of the second peak, denoted g_2, in the oxygen–oxygen pair-correlation function.[11] They also found a linear trend in the position of the first peak in the oxygen–oxygen pair-correlation function, denoted r_1, which was related to thermal expansion. Furthermore, they established an isosbestic point in the local oxygen–oxygen coordination number at 3.30 ± 0.05 Å, corresponding to an average number of 4.3 ± 0.2 oxygen atoms, for their experiments between 254 and 366 K. Pathak *et al.*[15] and Benmore *et al.*[16] extended the temperature range down to 235 and 244 K, respectively, and confirmed the isosbestic point to be 4.39 ± 0.15 oxygen atoms at 3.31 ± 0.05 Å and 4.2 ± 0.1 oxygen atoms at 3.26 Å, respectively. Both Pathak *et al.*[15] and Benmore *et al.*[16] found enhanced intermediate-range correlations for the fourth and fifth peaks in $g_{OO}(r)$ at $r \approx 9$ Å and $r \approx 11$ Å upon deep supercooling associated with the growth of a local tetrahedral network, which is distinctly different from that of hexagonal ice. Benmore *et al.*[16] highlighted the reduction of interstitial molecules[17] between the first and second coordination shell upon deep supercooling and argued that hexagons are still ill-defined in the low-density liquid that develops, although the second coordination shell implies local tetrahedral coordination. Pathak *et al.*[15] extended this argument and proposed that the low-density liquid contains clathrate-like structures making up pentamers.

Water also exists in three distinct vitreous forms,[1] known as low-density amorphous (LDA), high-density amorphous (HDA), and very high-density amorphous (VHDA) ice, with clear changes in local structure beyond density. Experimental observations[18] of an apparent first-order transition between LDA and HDA ice were the initial spark of water's polyamorphism over three decades ago. Loerting *et al.*[19] later found that isobaric heating of HDA ice above ~0.8 GPa (up to 160 K) produces VHDA ice that has ~9% higher density than HDA ice. The amorphous ices have clear differences in local structure beyond density[17,20,21] with most notably a shift of the first peak position (q_1) in the oxygen–oxygen structure factor from 1.71 Å^{-1} for LDA ice to $q_1 = 2.14$ Å^{-1} and $q_1 = 2.28$ Å^{-1} for HDA and VHDA ice, respectively.[21] Recently, the corresponding macroscopic liquid phases of a low-density liquid (LDL) and a high-density liquid (HDL) could be probed by exciting low-temperature-quenched HDA ice in vacuum into HDL and following the subsequent expansion in to LDL.[22] The two liquid phases are expected to interconvert with 1:1 population close to the Widom line.[23,24] The q_1 positions of both HDL and LDL are almost identical to HDA and LDA ice, respectively.

In this study, we further investigate the splitting of the principal maximum by evaporative cooling of micrometer-sized water droplets *in vacuo*, probed by WAXS using the ultrashort and ultrabright pulses produced at SwissFEL. Compared to previous studies at x-ray free-electron lasers,[9,11] we use an extended momentum transfer (q) range and an improved detector that reduces systematic errors at high q where the signal is weak. The high data quality allows us to accurately extract the position of the second peak in the principal doublet, denoted q_2, as a function of temperature. The positive derivative of the peak position with respect to temperature observed below 236 K cannot be explained by extrapolation of the trends in q_2 or r_1 observed at higher temperatures. Instead, we propose that the anomalous q_2 shift originates from that a repeat spacing in the tetrahedral network, associated with all correlations beyond the first shell in $g_{OO}(r)$, gives rise to a less dense local ordering that resembles that of LDA ice. Although our limited q range of 0.3–4.2 Å^{-1} does not allow direct Fourier inversion to real space, we show using combined data with Benmore *et al.*[16] that $g_{OO}(r)$ can be derived with reasonable accuracy beyond the first coordination shell. This highlights the richness of the structural information in the water principal structure factor doublet and explains its strong temperature dependence.

II. METHODS

A. WAXS measurements at SwissFEL

A series of diffraction patterns of supercooled water droplets were collected at the Bernina instrument[25] at SwissFEL at Paul Scherrer Institute (PSI) for different temperatures (228.5–268.0 K). Deionized water (Milli-Q, resistivity 18.2 MΩcm at 298 K) was injected into a vacuum chamber that can supercool droplets by evaporative cooling using a Rayleigh jet with a diameter of 10 μm. The nozzle was driven by a piezoelectric actuator and produced droplets in a uniform droplet train with a diameter of 15 μm and a velocity of 16.6 m/s. The droplet size was measured in vacuum by a microscope setup using stroboscopic LED illumination, synchronized with the piezoelectric actuator. The droplet temperature was estimated by Knudsen's theory of evaporation based on the kinetic theory of gases, which relates the travel time of the droplet in vacuum to the cooling rate caused by evaporation.[9,11] There has been a debate[26–28] about the accuracy of the droplet temperature estimated using Knudsen's theory of evaporation for micrometer-sized water droplets *in vacuo*. We estimate the absolute errors in temperature to be of the order of ±1 K (Table S1); see Ref. 10 for more details. The x-ray pulses had a photon energy of 9.55 keV with a bandwidth of 0.5% and a pulse energy of ~400 μJ and were generated at a repetition rate of 25 Hz. The focal spot size of the x-ray beam (FWHM) was 14 × 14 μm^2, which was measured by a knife-edge scan. The scattering patterns were recorded on a charge-integrating detector[25,29] (16 Mpixel JUNGFRAU, JF7) with a sample-to-detector distance of 12.57 cm,

covering a q range of 0.3–4.2 Å^{-1}, according to $q = 4\pi \sin(\theta/2)/\lambda$, where θ is the scattering angle from the incident beam and λ is the wavelength. The area of a pixel on the JF7 detector was 75 × 75 μm^2. To measure the photon intensity of the beam, an additional charge-integrating detector (1.5 Mpixel JUNGFRAU, JF3) was used.

B. Data analysis

To measure the true angular dependence of the intensity, the data have to be corrected for detector response and incident polarization, as well as geometrical effects of the detector.[30] Gain, pedestal, and geometrical assembly were done according to standard routines for the JUNGFRAU detector.[31] The center position of the x-rays and sample-detector distance were determined from concentric rings of a silver behenate calibration sample (Fig. S5). After correcting for polarization and variations in the solid angle, the intensity was normalized to the incident pulse energy, which was monitored on the calibration JF3 detector (I_0-measurement). Weak and strong x-ray shots with I_0-measurements below and above 0.5 standard deviations of the median, respectively, were disregarded from further analysis. To remove any effect of the energy spectrum variation, x-ray shots with a spectrum-weighted photon energy that deviated more than 3 eV from the median of the photon energy were also filtered out. The scattering patterns that were collected during the measurements were classified as hits or misses based on the angularly integrated intensity profiles. For hit selection, the average of the scattered intensities between 1.69 and 3.01 Å^{-1} was used as a metric, and four times the median of the averaged normalized intensity was taken as the hit threshold. Furthermore, any effect of ice in the droplets was removed by introducing a separate threshold to the angularly integrated averaged intensities. For the ice threshold, the maximum gradient of the normalized intensities for a q- range between 1 and 4.5 Å^{-1} was calculated, and 0.5 photon/pixel was taken as the threshold. The classified shots were subsequently averaged separately with respect to each class. The average of all misses with an averaged normalized intensity below the median was used to remove the background of the average of all hits. After applying all these corrections, the total structure factor of water was extracted by removing the molecular form factor contribution from the corrected intensities and normalizing by the modified atomic form factors (MAFFs), so that it will not contain any intramolecular structural contributions. This can be obtained through the following relation:[13]

$$S_{x-ray}(q) = \frac{NI_{x-ray}(q) - MFF(q)}{9[\sum_\alpha c_\alpha f_\alpha(q)]^2}, \tag{1}$$

where $I_{x-ray}(q)$ is the intensity of the x-ray shots, $MFF(q)$ is the molecular form factor of H_2O taken from the work of Wang *et al.*,[32] and c_α and f_α are the fraction coefficients and the modified atomic form factors[30] of oxygen and hydrogen, respectively. Compton scattering was subtracted from the experimental data by including it in the quantum-chemical estimate of $MFF(q)$. Furthermore, N is the constant that was used to normalize the x-ray intensity and is determined by the integral method,[33] which is based on the fact that no molecule can overlap,

$$N = \frac{\int_{q_{min}}^{q_{max}} \frac{q^2 MFF(q)}{[\sum_\alpha c_\alpha f_\alpha(q)]^2} dq - 2\pi^2 \rho(T)}{\int_{q_{min}}^{q_{max}} \frac{q^2 I_{x\text{-}ray}(q)}{[\sum_\alpha c_\alpha f_\alpha(q)]^2} dq}, \tag{2}$$

where q_{min} and q_{max} were chosen to be 0.5 and 3.7 Å^{-1}, respectively, and $\rho(T)$ is the temperature-dependent density of water estimated from an extrapolation of the experimental data taken from the work of Kell *et al.*[34] to lower temperatures. The truncation of data to 3.7 Å^{-1} did not give a significant shift in peak positions for a reference dataset[35] at room temperature measured up to 16 Å^{-1}. After proper normalization, $S_{x\text{-}ray}(q)$ was used to obtain the oxygen–oxygen structure factor (S_{OO}) by removing the intermolecular contributions of hydrogen. Since the contribution of the hydrogen–hydrogen structure factor (S_{HH}) to $S_{x\text{-}ray}(q)$ is less than 1%,[36] it was disregarded from our calculations. Following the procedure of Skinner *et al.*,[13] $S_{OO}(q)$ was obtained using the following relation:

$$S_{OO}(q) = \frac{S_{x-ray}(q) - w_{OH}(q) S_{OH}(q)}{w_{OO}(q)}, \tag{3}$$

where $S_{OH}(q)$ is the oxygen–hydrogen structure factor, $w_{OH}(q) = \frac{4 f_O(q) f_H(q)}{9[\sum_\alpha c_\alpha f_\alpha(q)]^2}$ is the oxygen–hydrogen weighting factor, and $w_{OO}(q) = \frac{f_O(q)^2}{9[\sum_\alpha c_\alpha f_\alpha(q)]^2}$ is the oxygen–oxygen weighting factor.

To find the q position of both peaks in $S_{OO}(q)$ for each temperature, partial derivation of the structure factors has been carried out with respect to q. Numerically, this is done using second-order accurate central differences for the inner points in the array and first-order forward or backward differences at the boundary points. Then, to get the peak positions, a linear regression has been done in the region of ±0.5 Å in $\Delta S_{OO}/\Delta q$ with data restricted to about q_1 ± 0.032 Å^{-1} and q_2 ± 0.05 Å^{-1} for the flatter maxima at high temperature. The intercepts of the partial derivatives show how the peaks change with respect to temperature to high accuracy. We estimate the error in peak positions of the principal doublet of $S_{OO}(q)$ through error propagation of the uncertainty in intercepts. Similarly, partial derivation of the structure factors was carried out with respect to temperature, indicating the structural change with temperature. The integral of the magnitude of the partial derivatives between 1.5 and 3.1 Å^{-1} was used as a metric for structural change, since it covers both peaks in the principal doublet of $S_{OO}(q)$ for which the temperature dependence is noticeable. In this case, the integral of the magnitude of the deviation of the scattering of data around a running mean of five data points (~0.04 Å^{-1}) over the same q range was used as an error metric. The standard deviations of the droplet diameter and velocity from the optical microscopic images were used to find the errors in temperatures, which then were propagated to find the errors in the temperature derivatives of peak positions.

C. Fourier inversion

The most direct way to understand changes in $S_{OO}(q)$ is to relate it to $g_{OO}(r)$ in real space through Fourier inversion[37] (sine transformation). Unfortunately, our limited q range of 0.3–4.2 Å^{-1} results in extreme broadening upon Fourier inversion to real space (Fig. S10).

Instead, we combine our experimental data below 3.3 Å^{-1} with high-resolution data of Benmore *et al.*[16] up to 20 Å^{-1} at 269 K according to the following relation:

$$g_{OO}(r) = 1 + \frac{1}{2\pi^2 r\rho_0}\int q[S_{OO}(q) - 1]M(q)\sin(qr)dq, \quad (4)$$

where $M(q)$ is a modification function of Slepian type to suppress Fourier artifacts (Figs. S8 and S9). Data were interpolated to the bins of Benmore *et al.*,[16] with a bin width of 0.025 Å^{-1}, prior to Fourier inversion to avoid bin-related artifacts. As shown in Fig. 4 and discussed in the work of Benmore *et al.*,[16] the high-resolution data mainly affect the first peak in $g_{OO}(r)$, whereas the principal maximum in $S_{OO}(q)$ gives rise to intermediate-range order. Experimental data were combined with high-resolution data at 244 K (Fig. S16) and 269 K (Fig. 5) to ensure that structural changes are not due to the reference data used for Fourier inversion. The peak positions r_n of the second, third, fourth, and fifth peaks were determined by the position of the intercepts in the first derivative calculated using linear regression. The corresponding amplitudes g_n of the second, third, fourth and fifth peaks were then determined by linear interpolation of $g_{OO}(r)$ at the peak positions. Furthermore, the experimental results and the temperature dependence of all peak parameters were compared to simulations using a polarizable water model,[38] the so-called inexpensive atomic multipole optimized energetics for biomolecular applications (iAMOEBA) force field, to describe the source of the drop in the q_2 position for lower temperatures. Details on the simulations and tabulated experimental data are also available in the supplementary material.

III. RESULTS

In this section, we present experimental results on the change in the oxygen–oxygen structure factor and, particularly, the second peak behavior upon supercooling. Figure 1 shows the oxygen–oxygen structure factor of water as a function of momentum transfer for different temperatures. It can be seen that upon supercooling, the first peak clearly shifts to lower values of q_1, whereas the second peak initially shifts to higher q_2 and then varies more subtly. We note that our data are consistent with the general trend of previous WAXS measurements[11,12,15,16] of water upon supercooling, except that a small local maximum exists at ~4 Å^{-1}. This is an artifact due to weak residual background scattering and occurs above the normalization range, which means it does not affect the accuracy of the data around the principal doublet. Similar to Benmore *et al.*,[16] we observe that the second peak increases strongly in amplitude, S_2, with decreasing temperature, reaching ~1.67 at 229 K. However, the high quality of the scattering data revealed a distinct trend for the second peak below 236 K (inset of Fig. 1) not seen in previous datasets, namely, the second peak moves back to lower q_2 values below 236 K. In Fig. 2, the temperature derivative of $S_{OO}(q)$ is shown as a function of temperature, which displays that the structural change accelerates upon deep supercooling. As in previous experiments,[9] a maximum is seen in the integral of $|\Delta S_{OO}(q)/\Delta T|$ at 229 K (Fig. 2 inset), which decays slightly for the last data point at lower temperature. This suggests an accelerated growth of local tetrahedral structures down to 229 K, which coincides with a maximum in volume[9] and entropy[10] fluctuations. We note that the signal-to-noise ratio gradually decreases below 235 K due to the smaller number of water shots at these temperatures, which is expected due to the steep increase in the nucleation rate.[39] Nevertheless, the temperature derivative of $S_{OO}(q)$, which enhances errors compared to its primitive function, showcases the high quality of our experimental data around the principal maximum.

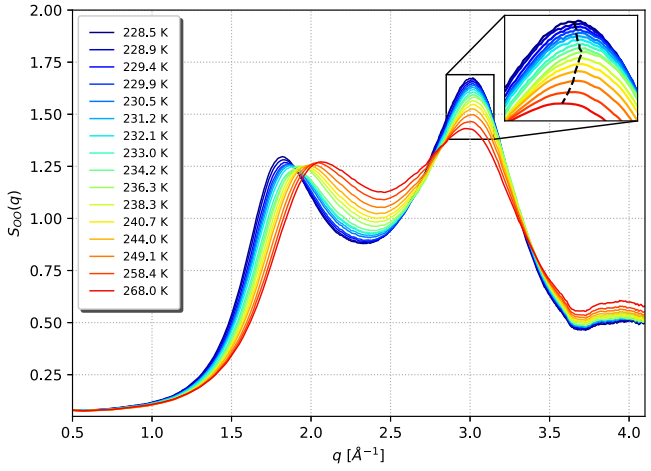

FIG. 1. Oxygen–oxygen structure factor (S_{OO}) of water as a function of momentum transfer (q) upon deep supercooling. Visual inspection of experimental data (inset) reveals a trend change in the shift of the second peak position (q_2) of the principal doublet as a function of temperature below ~236 K.

Figure 3 presents q_1 and q_2 as functions of temperature with their partial derivatives with respect to temperature as insets. q_1 decreases monotonically from 2.07 Å^{-1} at 268 K to 1.82 Å^{-1} at 229 K upon supercooling, whereas q_2 increases from 2.98 Å^{-1} at 268 K to 3.03 Å^{-1} at 236 K and then deviates from its monotonic behavior at high temperatures when it decreases to 3.01 Å^{-1} at 229 K. This is evident from the partial derivative of q_2 with respect to temperature [Fig. 3(a) inset], which changes sign at about 236 K and is beyond the uncertainty of the measurement. The data agree well, albeit a fairly constant shift, with previous $S_{OO}(q)$ measurements by Benmore *et al.*[16] down to 244 K and Pathak *et al.*[15] down to 235 K. The shift in q_2 is within the accuracy of our peak position determination, whereas the shift in q_1 is likely due to small systematic errors from the photon energy/detector distance calibration and the integral normalization. We note that the absolute position of q_1 and q_2 in our measurements is sensitive to the choice of background subtraction and hit selection, whereas the relative trend as a function of temperature is robust. This trend is highlighted in the partial derivatives with respect to temperature, which can be calculated numerically with high accuracy due to the high signal-to-noise ratio in our experimental data. It is quite unexpected to observe a maximum in q_2 upon deep supercooling, but a qualitatively similar behavior is seen for the iAMOEBA water model. When simulations are performed at 1000 atm, which exhibit significant volume and entropy fluctuations from the apparent diverging point (ADP) located at about 1700 atm and 180–190 K,[42] a maximum in q_2 is observed at about 210 K but less sharp in comparison to the current experimental data. The maximum is not observed in simulations at 1 atm (Fig. S4), which only give rise to an inflection point at a similar temperature. This suggests that the deviation in q_2 from a monotonically increasing trend is an anomalous behavior related to the growing fluctuations upon deep supercooling.

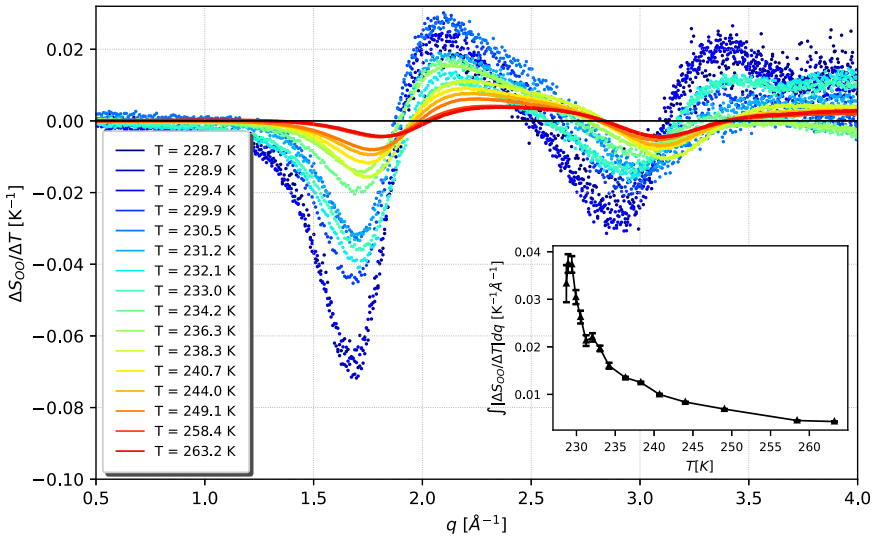

FIG. 2. Temperature derivative of $S_{OO}(q)$ as a function of momentum transfer (q). Upon deep supercooling, the magnitude in the structural change increases drastically (inset) with a maximum at 229 K that coincides with the maxima in volume and entropy fluctuations.

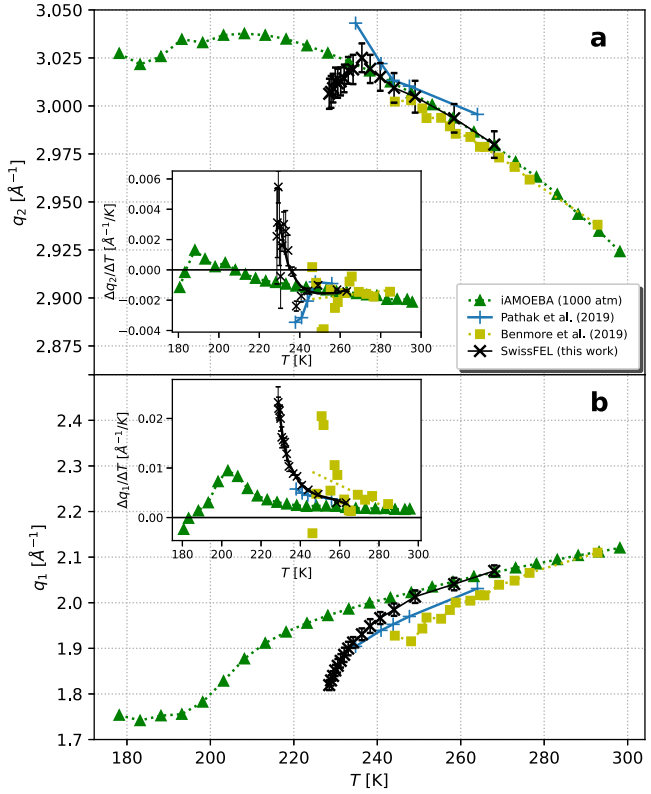

FIG. 3. Peak position of the (a) second (q_2) and (b) first (q_1) peaks of the principal doublet (black crosses) as a function of temperature (T) together with the iAMOEBA water model at 1000 atm (green triangles) and previous experimental data from Ref. 15 (blue crosses) and Ref. 16 (yellow squares). The insets show the partial derivative of q_2 and q_1, respectively, with respect to temperature (black solid line is a Savitzky–Golay filtering, and yellow dotted line is a linear fit that serves as guide to the eye). Error bars are calculated based on Gaussian error propagation, as described in Sec. II.

IV. DISCUSSION

It is well known that the principal maximum of $S_{OO}(q)$ of water at high temperature splits up into two peaks upon cooling[40,41] for which the first peak occurs at around $q_1 = 2$ Å^{-1} and the second peak occurs at around $q_2 = 3$ Å^{-1} at room temperature. Several interpretations have been made to explain the principal doublet of $S_{OO}(q)$ in terms of real-space structure. The peak split has been assigned to be related to the second nearest neighbor in the local water structure, since it correlates well with the tetrahedrality of water.[11,42] Benmore *et al.*[16] suggested a different view of the principal doublet in $S_{OO}(q)$, which reflects two periodic spacings in the hydrogen-bonded network associated with local tetrahedral ordering. They found that the second peak in $S_{OO}(q)$ dominates the coordination shells beyond the nearest neighbor with a direct correlation between their amplitudes (g_2, g_3, g_4, and g_5) and the increase in S_2. This suggests that a decrease in q_2 would be indicative of the periodic spacing $2\pi/q_2$ increasing, thus resulting in r_2, r_3, r_4, and r_5 increasing to larger values upon cooling below 236 K. In the following, we aim to test these different views by combining our experimental data with those of Benmore *et al.*[16] We then derive g_2, g_3, g_4, and g_5 down to 229 K and observe the origin of the change in sign of the temperature derivative of q_2.

We start by separating $g_{OO}(r)$ at 244 K from the work of Benmore *et al.*[16] into a product of the first peak and correlations at longer distances (Fig. S20a), including the second peak and intermediate-range order. We then invert each factor of the product to reciprocal space (Fig. S20b) with the original $S_{OO}(q)$ at 244 K being a convolution of the Fourier-transformed factors. This demonstrates that a peak in $S_{OO}(q)$ cannot be assigned to a peak in $g_{OO}(r)$. Instead, we propose to view the water structure factor as a sinc function (as established by the Debye scattering equation) from the sharp first peak in $g_{OO}(r)$ with intermediate-range order giving rise to distortions of the principal maximum of the structure factor and resulting in the doublet formation. It is quite remarkable that these structural distortions from intermediate-range order are contained to the principal maximum and do not affect the higher-order maxima in the

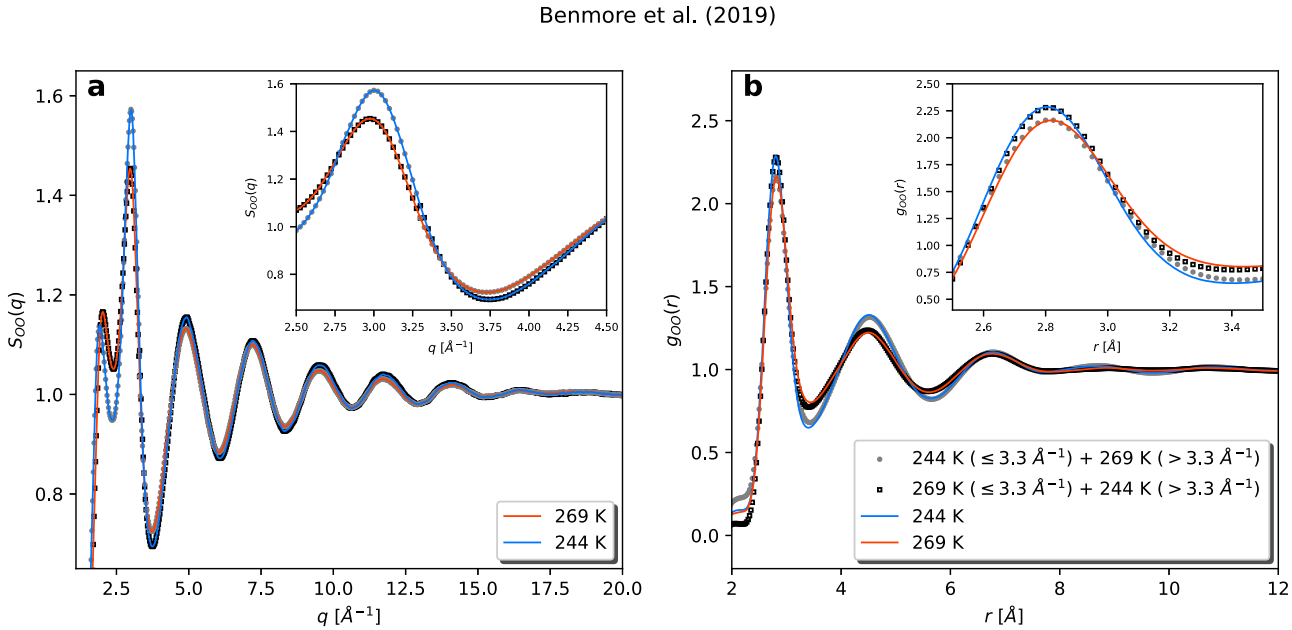

FIG. 4. Fourier inversion of x-ray scattering data from Ref. 16. The oxygen–oxygen structure factor (S_{OO}) of water at 244 K (blue solid line) and 269 K (red solid line) in (a) is inverted to the oxygen–oxygen pair-correlation function (g_{OO}) in (b) using a modification function of Slepian type (supplementary material). To highlight the effect of the principal maximum in $S_{OO}(q)$, data at 244 K are combined above 3.3 Å^{-1} with data at 269 K (gray filled circles) and vice versa (black hollow squares). It is evident from the combined data that changes in the principal maximum in $S_{OO}(q)$ dominate the structural changes beyond the first coordination shell, including the intermediate-range order, whereas the amplitude of the higher-order maxima in $S_{OO}(q)$ determines sharpness of the first peak in $g_{OO}(r)$.

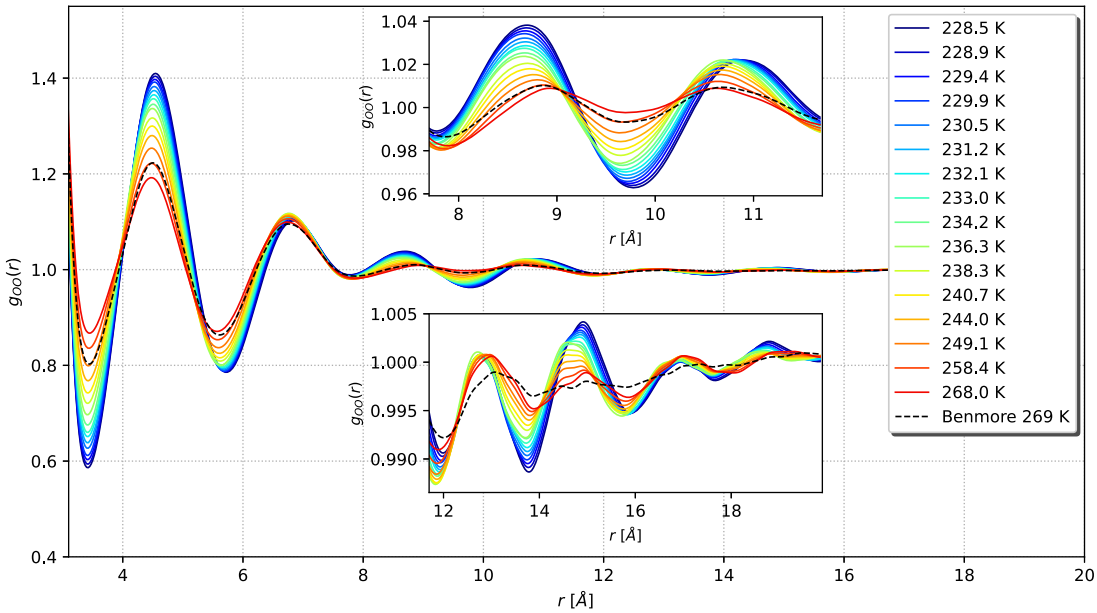

FIG. 5. Fourier inversion of our experimental data at $q \leq 3.3$ Å^{-1} combined with high-resolution x-ray scattering data from Ref. 16 at 269 K. Oxygen–oxygen pair-correlation function (g_{OO}) beyond the first coordination shell is shown for all temperatures and compared with the original reference data from Ref. 16 at 269 K (black dashed line). The upper inset highlights structural changes in the fourth and fifth peaks, whereas the lower inset shows long-range ordering beyond 12 Å. The same modification function as used in Fig. 4 was used for Fourier inversion of all combined data; see Sec. II for further details.

structure factor. This may be understood in terms of the limited q range of the Fourier transform of the intermediate-range order and the rapidly decaying amplitude of the higher-order maxima of the sinc function. Conversely, the higher-order maxima in the structure factor define the sharpness of the first coordination shell in $g_{OO}(r)$. This is showcased in Fig. 4, which shows the Fourier inversion of experimental structure factor data from the work of Benmore *et al.*[16] at 244 K (blue solid line) and 269 K (red solid line). We can combine experimental data at 244 K below 3.3 Å^{-1} with data at 269 K above 3.3 Å^{-1} (gray filled circles) and vice versa (black hollow squares) and compare the resulting $g_{OO}(r)$ upon Fourier inversion. It is evident from the combined data that changes in the principal maximum in $S_{OO}(q)$ dominate the structural changes beyond the first coordination shell, including the intermediate-range order, whereas the amplitude of the higher-order maxima in $S_{OO}(q)$ clearly determines the height of the first peak in $g_{OO}(r)$.

Based on this revelation, we combine our experimental data below 3.3 Å^{-1} with the experimental data from the work of Benmore *et al.*[16] at 269 K and obtain $g_{OO}(r)$ through Fourier inversion. This circumvents the Fourier artifacts or extreme broadening that would occur when inverting experimental data of such limited q range (Fig. S10) but makes the resulting $g_{OO}(r)$ unreliable for the first coordination shell. We chose a cutoff of 3.3 Å^{-1} as this is where $S_{OO}(q)$ is close to 1, and our data is almost isosbestic, which minimizes systematic errors due to stitching. We use a modification function of

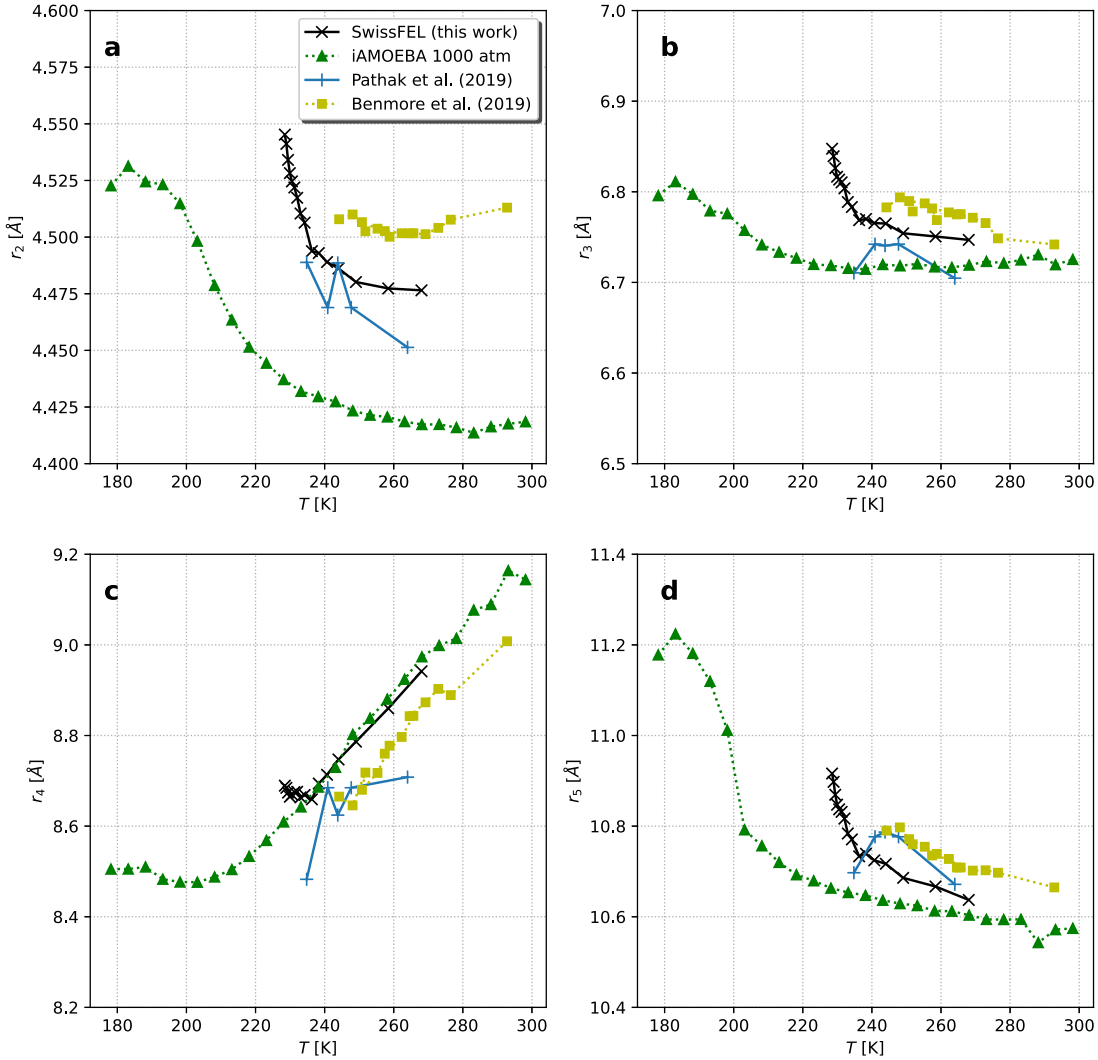

FIG. 6. Peak positions of the (a) second (r_2), (b) third (r_3), (c) fourth (r_4), and (d) fifth (r_5) peaks in the oxygen–oxygen pair-correlation function from our experimental data combined with high-resolution x-ray scattering data from Ref. 16 at 269 K. Our data (black crosses) are compared with peak positions of the iAMOEBA water model at 1000 atm (green triangles) and previous experimental data from Ref. 15 (blue crosses) and Ref. 16 (yellow squares). Our SwissFEL data and data from Ref. 16 have been converted with an identical modification function of Slepian type (supplementary material), whereas data from Ref. 15 use a modified Lorch function.

Slepian type that effectively removes Fourier ripples due to q truncation but slightly dampens the correlations in the first and second coordination shell. Figure 5 shows the resulting $g_{OO}(r)$ for the second shell and outward with the conversion of the original data from the work of Benmore *et al.*[16] (black dashed line) as the reference. The most dominating change upon cooling is the sharpening of the second shell at 4.5 Å and reduction of interstitials at about 3.3 Å, as highlighted in previous studies,[11,16] but we also see an increased correlation in the fourth and fifth shell at 8.8 and ~11 Å, respectively, and the emergence of an unprecedented sixth shell at ~15 Å upon deep supercooling, similar to LDA ice.[21] The general trend upon supercooling resembles a continuous transformation from HDA to LDA ice.

We note that the reference data from the work of Benmore *et al.*[16] at 269 K overlap best with the combined data at 258 K, whereas changing reference data to those of Benmore *et al.*[16] at 244 K gives best overlap with the combined data at 238 K (Fig. S16). This suggests systematic errors between the datasets that resemble temperature changes of ≤10 K. Nevertheless, the relative trends in the combined dataset are robust and do not depend on the temperature of the reference data used for stitching (Fig. S19). The oxygen–oxygen coordination number can be calculated from $g_{OO}(r)$ combined with experimental data from the work of Benmore *et al.*[16] (Fig. S15) as well as directly inverted experimental data (Fig. S11), which suffer from extreme broadening. In both cases, the oxygen–oxygen coordination number shows an isosbestic

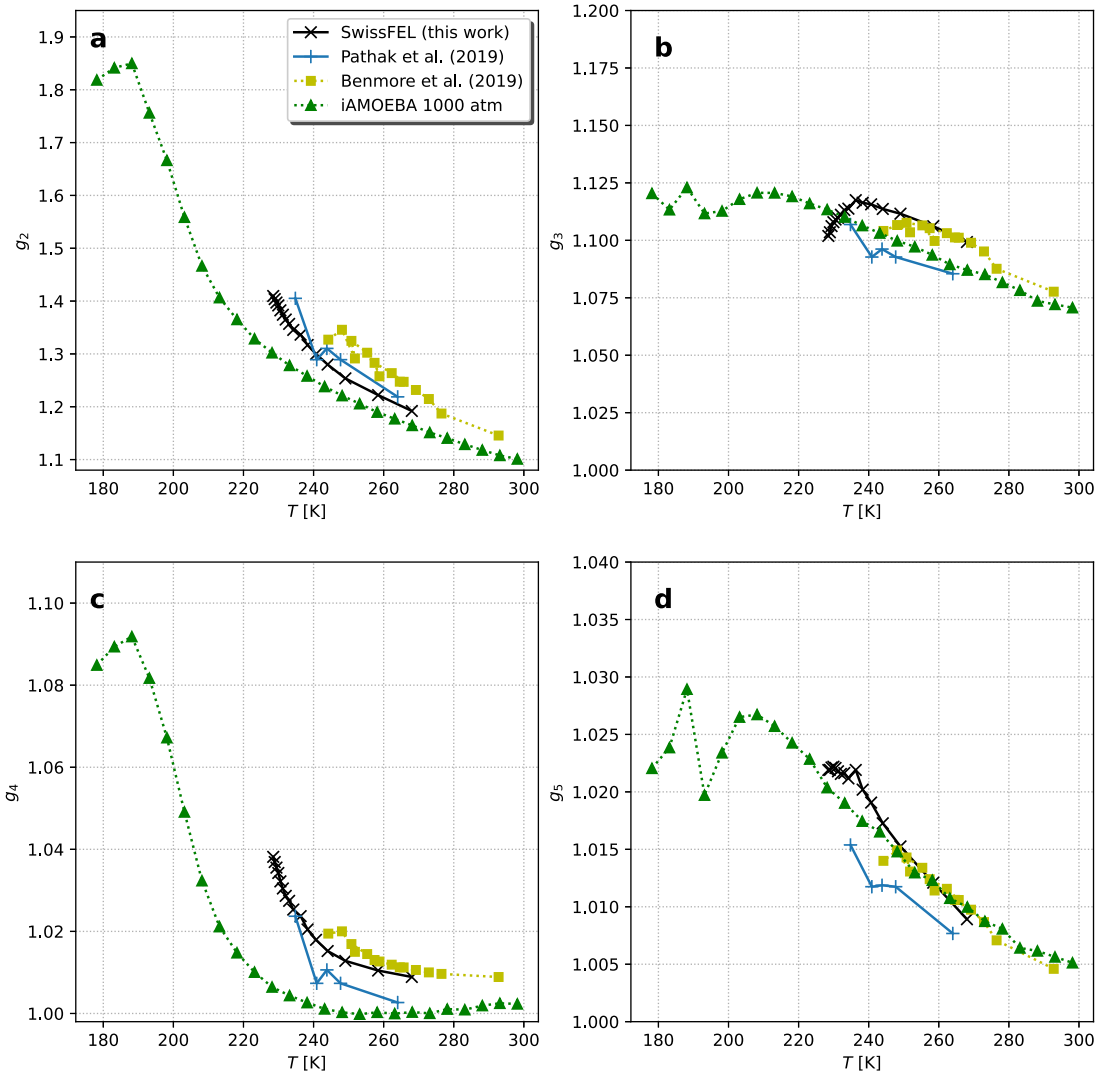

FIG. 7. Peak amplitudes of the (a) second (g_2), (b) third (g_3), (c) fourth (g_4), and (d) fifth (g_5) peaks in the oxygen–oxygen pair-correlation function from our experimental data combined with high-resolution x-ray scattering data from Ref. 16 at 269 K. Our data (black crosses) are compared with peak positions of the iAMOEBA water model at 1000 atm (green triangles) and previous experimental data from Ref. 15 (blue crosses) and Ref. 16 (yellow squares). Our SwissFEL data and data from Ref. 16 have been converted with an identical modification function of Slepian type (supplementary material), whereas data from Ref. 15 use a modified Lorch function.

point around 3.1 Å, which is shorter than previous studies[12,15,16] ranging from 3.26–3.31 Å. This may be due to the suppressed amplitude in the first coordination shell (g_1), which is expected to increase significantly upon deep supercooling and increase the oxygen–oxygen coordination number at short distances as temperature is reduced.

Figures 6 and 7 present the peak positions and amplitudes, respectively, of the second, third, fourth, and fifth peaks in $g_{OO}(r)$ for the combined data using reference data at 269 K and compare them with the experimental data from the work of Benmore *et al.*[16] and Pathak *et al.*[15] and simulations at 1000 atm using the iAMOEBA water model. The experimental data from the work of Benmore *et al.*[16] have been converted with the same type of modification function as the combined data, whereas Pathak *et al.*[15] used a modified Lorch function that gives slightly sharper peaks but also slightly more Fourier ripples (Figs. S8 and S9). The most striking feature in the combined data is that all peak positions move to longer distances below 236 K, a trend that is only qualitatively reproduced at lower temperatures by the iAMOEBA water model at 1000 atm. Simultaneously, even peaks increase strongly in amplitude, whereas odd peaks decrease or flatten. The elongated peak positions below 236 K suggest that a repeat spacing in the tetrahedral network, associated with all peaks in $g_{OO}(r)$, gives rise to a less dense local ordering. More pronounced low-density structural motifs in the liquid may explain the steep increase in the nucleation rate upon deep supercooling, but as previous studies[15,16,21,43] have noted, the third peak in ice Ih around ~5.2 Å is absent in metastable water. This means that six-membered rings with tetrahedrally coordinated para-oxygens must be rare in the liquid even upon deep supercooling. The opposite behavior in the peak amplitude between the third and fourth peak appears at first counterintuitive but could be understood if the peaks are dominated by various local structures. According to the latest experimental data on amorphous ices by Mariedahl *et al.*,[21] HDA ice has a slightly larger amplitude for the third peak than that for LDA ice, whereas LDA ice has much larger amplitude for the fourth peak. The peak behavior for the combined data is thus consistent with a conversion of high-density to low-density local structures that resemble those of amorphous ices. Based on this conversion, r_4 is thought to be sensitive to the ratio of low-density and high-density local structures in the liquid,[15] where lower r_4 values indicate more low-density local structures. This rule of thumb appears to break down below 236 K when r_4 increases on further cooling.

One can discuss what would be the best representation of local structures in liquid water. It has been assumed that fragmental configurations of clathrate-like structures containing a mixture of five- and six-membered rings of hydrogen-bonded water molecules become more abundant upon supercooling.[44–47] Simultaneously, tetrahedrality increases with higher population of low-density local structures.[15,48,49] The fact that all peak positions move to longer distances below 236 K suggests that tetrahedrally coordinated pentamers and hexamers fuse into larger low-density regions. Camisasca *et al.*[43] investigated the feasibility of chain-like hydrogen-bonded structures and fused dodecahedra as representations of high-density and low-density local structures, respectively. The second and fourth peak positions of the fused dodecahedra match well with those of liquid water, whereas the third and fifth peak positions are 0.5–1 Å shorter than those presented in Fig. 6. This could be due to that fused dodecahedra are an inadequate representation of the connectivity between ring-like low-density structures in the liquid or that other high-density structures alter the correlations for the third and fifth peaks without giving significant contributions to the fourth peak.

V. CONCLUSIONS

In this study, we investigated the structural changes of water upon deep supercooling using evaporative cooling of micrometer-sized droplets and WAXS at SwissFEL. We found that the structure of water demonstrates an anomalous behavior for the second peak of $S_{OO}(q)$ below 236 K, which is correlated with the intermediate-range order in $g_{OO}(r)$. This new observation was analyzed and tested through Fourier inversion of our experimental data below 3.3 $Å^{-1}$ with the experimental data from the work of Benmore *et al.*[16] at 244 and 269 K. The resulting $g_{OO}(r)$ was unreliable for the first coordination shell, which is defined by the higher-order maxima of $S_{OO}(q)$, but showed a sharpening of the second shell at 4.5 Å and reduction of interstitials at about 3.3 Å. It also revealed increased intermediate-range ordering out to an unprecedented sixth shell at ~15 Å upon deep supercooling. These changes resemble a continuous transformation toward LDA ice, indicating that tetrahedrally coordinated low-density configurations rapidly expand in size upon supercooling. Below 236 K, when q_2 decreases, all peak positions (r_2, r_3, r_4, and r_5) elongate upon further cooling. This suggests that a repeat spacing in the tetrahedral network, associated with all peaks in $g_{OO}(r)$, gives rise to a less dense local ordering. iAMOEBA simulations at 1000 atm support that r_2, r_3, r_4, and r_5 increase when q_2 decreases upon deep supercooling, although they vastly underestimate the rate of change with temperature. The oxygen–oxygen coordination number showed an isosbestic point at about ~3.1 Å, a shorter distance than previous studies, which we believe is caused by the suppressed first peak amplitude using our combined data approach. This could be tested by WAXS experiments with an extended q range that allow direct Fourier inversion to real space and can accurately determine the first coordination shell in $g_{OO}(r)$ below 236 K.

Fragmental configurations of clathrate-like structures with an abundance of pentamers give a better representation of the low-density liquid structure than ice-like hexamers. The collapse of these pentamer-based structures in the liquid phase at even lower temperatures (or longer time scales) results in that hexagonal or cubic ice is rapidly formed, because six-membered rings can then join other coordinated oxygens and quickly form larger ice clusters. This would suggest that water's strong metastability stems from low-density local structures that are distinctly different from hexagonal ice. It would be interesting to perform vibrational spectroscopy studies upon deep supercooling in order to find out more about the effect of collective motions and their connection to the ordering of the low-density local structures that develop at this temperature region.

SUPPLEMENTARY MATERIAL

The supplementary material includes five sections with 19 supporting figures and supplementary texts on the iAMOEBA water model (pp. 1–5), sample-detector calibration (p. 6), $S(q)$ normalization (pp. 7 and 8), Fourier inversion of $S(q)$ to $g(r)$ (pp. 9–19), and inversion of different peaks in $g(r)$ (p. 20). It also includes a table on

q_1 and q_2 positions and the corresponding errors (p. 21), as well as a spreadsheet with the full $S_{OO}(q)$ data for all recorded temperatures.

ACKNOWLEDGMENTS

This work was supported by a European Research Council Advanced Grant under Project No. 667205 and the Swedish National Research Council (Starting Grant No. 2017-05128). K. Amann-Winkel acknowledges funding from the Ragnar Söderbergs Stiftelse, and K. H. Kim and C. Yang were supported by the National Research Foundation of Korea (NRF) grant funded by the Korean government (MSIT) (Grant No. 2020R1A5A1019141). The experiments were performed at beamline BERNINA of SwissFEL (Proposal No. p17743) funded by the Paul Scherrer Institute, Switzerland, with supporting experiments performed at beamline BL3 of SACLA (Proposal No. 2018A8063), Japan. We appreciate the support of the SACLA staff for our pre-study. We thank L.-P. Wang for providing iAMOEBA radial distribution data and C. Benmore for providing the x-ray scattering data.

AUTHOR DECLARATIONS

Conflict of Interest

The authors declare no conflict of interest.

DATA AVAILABILITY

The data that support the findings of this study are available within the article and its supplementary material.

REFERENCES

[1] P. G. Debenedetti, "Supercooled and glassy water," J. Phys.: Condens. Matter **15**, R1669–R1726 (2003).
[2] P. H. Poole, F. Sciortino, U. Essmann, and H. E. Stanley, "Phase-behavior of metastable water," Nature **360**, 324–328 (1992).
[3] M. A. Anisimov *et al.*, "Thermodynamics of fluid polyamorphism," Phys. Rev. X **8**, 011004 (2018).
[4] D. T. Limmer and D. Chandler, "The putative liquid-liquid transition is a liquid-solid transition in atomistic models of water," J. Chem. Phys. **135**, 134503 (2011).
[5] D. T. Limmer and D. Chandler, "The putative liquid-liquid transition is a liquid-solid transition in atomistic models of water. II," J. Chem. Phys. **138**, 214504 (2013).
[6] D. T. Limmer and D. Chandler, "Theory of amorphous ices," Proc. Natl. Acad. Sci. U. S. A. **111**, 9413–9418 (2014).
[7] Y. Xie, K. F. Ludwig, G. Morales, D. E. Hare, and C. M. Sorensen, "Noncritical behavior of density fluctuations in supercooled water," Phys. Rev. Lett. **71**, 2050–2053 (1993).
[8] C. Huang *et al.*, "The inhomogeneous structure of water at ambient conditions," Proc. Natl. Acad. Sci. U. S. A. **106**, 15214–15218 (2009).
[9] K. H. Kim *et al.*, "Maxima in the thermodynamic response and correlation functions of deeply supercooled water," Science **358**, 1589–1593 (2017).
[10] H. Pathak *et al.*, "Enhancement and maximum in the isobaric specific heat capacity measurements of deeply supercooled water using ultrafast calorimetry," Proc. Natl. Acad. Sci. U. S. A. **118**, e2018379118 (2021).
[11] J. A. Sellberg *et al.*, "Ultrafast X-ray probing of water structure below the homogeneous ice nucleation temperature," Nature **510**, 381–384 (2014).
[12] L. B. Skinner, C. J. Benmore, J. C. Neuefeind, and J. B. Parise, "The structure of water around the compressibility minimum," J. Chem. Phys. **141**, 214507 (2014).
[13] L. B. Skinner *et al.*, "Benchmark oxygen-oxygen pair-distribution function of ambient water from x-ray diffraction measurements with a wide Q-range," J. Chem. Phys. **138**, 074506 (2013).
[14] A. K. Soper, "The radial distribution functions of water as derived from radiation total scattering experiments: Is there anything we can say for sure?," ISRN Phys. Chem. **2013**, 279463.
[15] H. Pathak *et al.*, "Intermediate range O–O correlations in supercooled water down to 235 K," J. Chem. Phys. **150**, 224506 (2019).
[16] C. Benmore, L. C. Gallington, and E. Soignard, "Intermediate range order in supercooled water," Mol. Phys. **117**, 2470–2476 (2019).
[17] J. L. Finney, A. Hallbrucker, I. Kohl, A. K. Soper, and D. T. Bowron, "Structures of high and low density amorphous ice by neutron diffraction," Phys. Rev. Lett. **88**, 225503 (2002).
[18] O. Mishima, L. D. Calvert, and E. Whalley, "An apparently first-order transition between two amorphous phases of ice induced by pressure," Nature **314**, 76–78 (1985).
[19] T. Loerting, C. Salzmann, I. Kohl, E. Mayer, and A. Hallbrucker, "A second distinct structural 'state' of high-density amorphous ice at 77 K and 1 bar," Phys. Chem. Chem. Phys. **3**, 5355–5357 (2001).
[20] J. L. Finney *et al.*, "Structure of a new dense amorphous ice," Phys. Rev. Lett. **89**, 205503 (2002).
[21] D. Mariedahl *et al.*, "X-ray scattering and O–O pair-distribution functions of amorphous ices," J. Phys. Chem. B **122**, 7616–7624 (2018).
[22] K. H. Kim *et al.*, "Experimental observation of the liquid–liquid transition in bulk supercooled water under pressure," Science **370**, 978–982 (2020).
[23] K. T. Wikfeldt, C. Huang, A. Nilsson, and L. G. M. Pettersson, "Enhanced small-angle scattering connected to the Widom line in simulations of supercooled water," J. Chem. Phys. **134**, 214506 (2011).
[24] K. T. Wikfeldt, A. Nilsson, and L. G. M. Pettersson, "Spatially inhomogeneous bimodal inherent structure in simulated liquid water," Phys. Chem. Chem. Phys. **13**, 19918–19924 (2011).
[25] G. Ingold *et al.*, "Experimental station Bernina at SwissFEL: Condensed matter physics on femtosecond time scales investigated by X-ray diffraction and spectroscopic methods," J. Synchrotron Radiat. **26**, 874–886 (2019).
[26] C. Goy *et al.*, "Shrinking of rapidly evaporating water microdroplets reveals their extreme supercooling," Phys. Rev. Lett. **120**, 015501 (2018).
[27] F. Caupin *et al.*, "Comment on 'Maxima in the thermodynamic response and correlation functions of deeply supercooled water,'" Science **360**, eaat1634 (2018).
[28] K. H. Kim *et al.*, "Response to Comment on 'Maxima in the thermodynamic response and correlation functions of deeply supercooled water,'" Science **360**, eaat1729 (2018).
[29] C. J. Milne *et al.*, "SwissFEL: The Swiss X-ray free electron laser," Appl. Sci. **7**, 720 (2017).
[30] G. Hura, J. M. Sorenson, R. M. Glaeser, and T. Head-Gordon, "A high-quality x-ray scattering experiment on liquid water at ambient conditions," J. Chem. Phys. **113**, 9140–9148 (2000).
[31] S. Redford *et al.*, "Operation and performance of the JUNGFRAU photon detector during first FEL and synchrotron experiments," J. Instrum. **13**, C11006 (2018).
[32] J. Wang, A. N. Tripathi, and V. H. Smith, "Chemical binding and electron correlation effects in x-ray and high energy electron scattering," J. Chem. Phys. **101**, 4842–4854 (1994).
[33] J. Krogh-Moe, "A method for converting experimental X-ray intensities to an absolute scale," Acta Crystallogr. **9**, 951–953 (1956).
[34] G. S. Kell, "Density, thermal expansivity, and compressibility of liquid water from 0° to 150° C: Correlations and tables for atmospheric pressure and saturation reviewed and expressed on 1968 temperature scale," J. Chem. Eng. Data **20**, 97–105 (1975).
[35] C. Huang *et al.*, "Wide-angle X-ray diffraction and molecular dynamics study of medium-range order in ambient and hot water," Phys. Chem. Chem. Phys. **13**, 19997–20007 (2011).
[36] Z. Su and P. Coppens, "Relativistic X-ray elastic scattering factors for neutral atoms Z = 1–54 from multiconfiguration Dirac–Fock wavefunctions in the 0–12 $Å^{-1}$ $\sin\theta/\lambda$ range, and six-Gaussian analytical expressions in the 0–6 $Å^{-1}$ range," Acta Crystallogr., Sect. A: Found. Crystallogr. **53**, 749–762 (1997).
[37] J. Waser and V. Schomaker, "The Fourier inversion of diffraction data," Rev. Mod. Phys. **25**, 671–690 (1953).

[38]L.-P. Wang *et al.*, "Systematic improvement of a classical molecular model of water," J. Phys. Chem. B **117**, 9956–9972 (2013).
[39]H. Laksmono *et al.*, "Anomalous behavior of the homogeneous ice nucleation rate in 'no-man's land,'" J. Phys. Chem. Lett. **6**, 2826–2832 (2015).
[40]Y. S. Badyal *et al.*, "Electron distribution in water," J. Chem. Phys. **112**, 9206–9208 (2000).
[41]A. H. Narten and H. A. Levy, "Liquid water: Molecular correlation functions from X-ray diffraction," J. Chem. Phys. **55**, 2263 (1971).
[42]H. Pathak *et al.*, "The structural validity of various thermodynamical models of supercooled water," J. Chem. Phys. **145**, 134507 (2016).
[43]G. Camisasca, D. Schlesinger, I. Zhovtobriukh, G. Pitsevich, and L. G. M. Pettersson, "A proposal for the structure of high- and low-density fluctuations in liquid water," J. Chem. Phys. **151**, 034508 (2019).
[44]H. Yokoyama, M. Kannami, and H. Kanno, "Existence of clathrate-like structures in supercooled water: X-Ray diffraction evidence," Chem. Phys. Lett. **463**, 99–102 (2008).
[45]J. Russo and H. Tanaka, "Understanding water's anomalies with locally favoured structures," Nat. Commun. **5**, 3556 (2014).
[46]M. Mandziuk, "From the trimer, through the pentamer, to liquid water," J. Mol. Struct. **1177**, 168–176 (2019).
[47]B. Santra, R. A. DiStasio, F. Martelli, and R. Car, "Local structure analysis in *ab initio* liquid water," Mol. Phys. **113**, 2829–2841 (2015).
[48]A. Perera, "On the microscopic structure of liquid water," Mol. Phys. **109**, 2433–2441 (2011).
[49]C. Lin, J. S. Smith, S. V. Sinogeikin, and G. Shen, "Experimental evidence of low-density liquid water upon rapid decompression," Proc. Natl. Acad. Sci. U. S. A. **115**, 2010–2015 (2018).